Detecting RyR clusters with CaCLEAN: influence of spatial distribution and structural heterogeneity

David Ladd[1*], Agne Tilunaite[2], Christian Soeller[3], H. Llewelyn Roderick[4], Edmund Crampin[2], Vijay Rajagopal[5]

***For correspondence:** david.ladd@unimelb.edu.au

Present address: [§]Systems Biology Lab, Department of Biomedical Engineering, University of Melbourne, Australia

[1]Systems Biology Lab, Department of Biomedical Engineering, University of Melbourne, Australia; [2]Systems Biology Lab, School of Mathematics and Statistics, University of Melbourne, Australia; [3]The Soeller Lab, Living Systems Institute, University of Exeter, United Kingdom; [4]Laboratory of Experimental Cardiology, Department of Cardiovascular Sciences, KU Leuven, Belgium; [5]Cell Structure and Mechanobiology Group, Department of Biomedical Engineering, University of Melbourne, Australia

Abstract In cardiomyocytes, the coordinated release of calcium ions from intracellular stores through ryanodine receptor (RyR) clusters is key to the generation of a calcium transient and induction of contraction. Recently, a deconvolution algorithm from radio astronomy was adapted and applied to analysis of calcium fluorescence imaging of cardiomyocytes. The algorithm, CaCLEAN, showed potential in revealing both the spatial locations of RyR clusters and their functional response in living cells. However, whether the RyR clusters identified by CaCLEAN analysis of the imaging data were true or false positives remained unvalidated in the absence of ground truth values. In this work, a structurally realistic finite element model was developed to simulate reaction-diffusion of calcium emanating from RyR clusters during the rising phase (first 30 ms) of the calcium transient. The effect of two sets of factors were examined with the model: (1) the number and spacing of simulated RyR clusters and (2) the effect of mitochondria acting as barriers to diffusion. Confocal fluorescence microscopy images were simulated from the model results and analysed using CaCLEAN. The performance of CaCLEAN was found to be sensitive to cluster spacing and distance from the imaging plane. In a case with sparsely-packed clusters, detection recall and precision were 0.82 for clusters up to 610 nm from the imaging plane; in a densely-packed cluster case, recall and precision were 0.69 for clusters up to 280 nm from the imaging plane. Users interested in applying CaCLEAN to their data should therefore consider the likely density of cluster distributions and the trade-off between precision and recall when determining the maximum relevant depth of RyR clusters in their application.

Introduction

Each heartbeat is induced by a flood of calcium (Ca2+) from the sarcoplasmic reticulum (SR), into the cytosol. This release of Ca2+ through clusters of ryanodine receptors (RyRs) raises the bulk cytosolic [Ca2+] concentration from 0.1 μM to ~1 μM within 30 ms and results in exposing of cross-bridge binding sites on the actin filaments, facilitating the cellular contractions that compose a heartbeat (***Bers, 2002***). Confocal (***Soeller and Cannell, 2002***) and super-resolution (***Hou et al.,***

2015) microscopy imaging of immuno-labelled cardiac tissue preparations has revealed the spatial organisation of RyR clusters, but measurements from fixed-tissues lack the ability to provide insights into functional response.

Tian et al. (***Tian et al., 2017***) recently proposed an adaption of the CLEAN method from radio astronomy (***Högbom, 1974***) to detect Ca2+ release sites from fluorescence confocal imaging of live cardiomyocytes. Using this algorithm (CaCLEAN) the authors demonstrated the possibility of determining the time-dependent functional response in live cell preparations using widely available experimental methods. Further, if proven in this context, similar methods may extend to any cellular process that can be approximated as an impulse response of a collection of point sources in a fluorescence microscopy signal.

Several questions remain however regarding the suitability and performance of CaCLEAN. In their original article, ***Tian et al.*** (***2017***) state that based on analysis of two Ca2+ transients with varying distance and convolved noise, CaCLEAN is able to resolve local transients with centres 1 μm apart. The authors deem a 1 μm minimum cluster spacing reasonable on the basis that the mean distance between RyR clusters was previously reported as 1.02 μm (***Soeller et al., 2007***). However, the cited measurement combines clusters within the same z-disk and those spanning separate z-disks. Clusters within a given z-disk are more closely packed, as apparent from the 0.66 μm nearest neighbour distance reported in the same study (***Soeller et al., 2007***). In the longitudinal orientation typical of experimental preparations of cardiomyocytes (as simulated below in ***Figure 3***A), this results in the presence of inter-cluster spacings below 1 μm in the imaging plane (i.e., along the y-axis of each z-disk in ***Figure 3***A) and in the through-imaging-plane depth.

Further complicating detection is that, compared to the near-vacuum between celestial objects, the diffusive volume between clusters of RyRs in cardiomyocytes is heterogeneous, consisting primarily of myofibrils and mitochondria. This is relevant to the local distribution of diffusing Ca2+: while homologues of cell membrane Ca2+ transport channels exist on mitochondria and exhibit a modest buffering effect, Ca2+ flux between the cytosol and intra-mitochondrial space is negligible compared to other cytosolic Ca2+ pathways under physiological conditions (***Williams et al., 2013***). Given this potential barrier-like effect of mitochondria to diffusing Ca2+, we hypothesized that Ca2+ reflecting against mitochondria could impact the detection performance of CaCLEAN.

In order to test the performance of CaCLEAN, we developed a spatially detailed computational model of an eight-sarcomere section of a cardiomyocyte, which we use to simulate reaction-diffusion of Ca2+ emanating from RyR clusters during the rising phase (first 30 ms) of the Ca2+ transient. Fluorescence microscopy data was simulated from this model and analysed with CaCLEAN. This allowed for the establishment of ground truth values for RyR cluster firing locations and assessment of performance in terms of true positives (hits), false negatives (misses), and false positives (algorithmic artefacts).

Our findings indicate that the presence of mitochondria only marginally impacts the performance of CaCLEAN. However, inter-RyR cluster spacing has a significant effect on detection performance and how far from the imaging plane clusters may be accurately detected. We estimate the accuracy and precision of the algorithm as between 69-82%, depending on the density of cluster locations and their distance from the imaging plane.

Results

Simulating microscopy data allows for assessment of detection performance with known ground truth values

An eight-sarcomere, spatially detailed, finite element (FE) computational model of an eight sarcomere section of a cardiomyocyte was constructed to test the precision and recall of CaCLEAN in detecting RyR clusters. The influence of mitochondria and the spatial arrangement of RyR clusters on the performance of CaCLEAN were studied. This resulted in four model permutations:

1. CASE 1 (high cluster density, no mitochondria): A case with high cluster density (N=984, 123

clusters per z-disk) based on statistical analysis of nearest neighbour distributions of clusters from immunolabeled confocal microscopy data (***Figure 1***B).

2. CASE 2 (low cluster density, no mitochondria): A case with a relatively lower cluster density (N=408 or 51 per z-disk) and an additional constraint of a minimum spacing of 1 μm spacing between cluster centers.
3. CASE 3 (high cluster density, with mitochondria): Mitochondrial regions (***Figure 1***C) were included within the computational model, acting as diffusion barriers. RyR cluster distributions were defined as in case 1.
4. CASE 4 (low cluster density, with mitochondria): Mitochondrial regions were included; RyR cluster distributions were defined as in case 2.

In the three-dimensional FE model, the fluorescence-bound Ca2+ (FCa) field at a given point was determined by the time-dependent reaction-diffusion from the surrounding cluster sources (see ***Figure 1***E). The FCa field was then interpolated onto a regular grid (see ***Figure 2***A) and temporally downsampled to 5 ms intervals. The FCa field was then convolved in three dimensions with a point spread function (PSF, ***Figure 2***B) to simulate optical blurring and light noise (SNR=100) was added. This dataset was then resampled at 215 nm resolution in two dimensions at 22 equidistant slices as indicated in ***Figure 2***C to obtain simulated images that mimic fast 2D confocal images obtained in typical experiments.

The resulting time-dependent, simulated confocal fluorescence microscopy images at each slice (***Figure 3***A) were then analysed with CaCLEAN to produce maps (***Figure 3***B), which were then segmented into individual clusters (***Figure 3***C). To measure algorithm performance we conducted a statistical classification (***Figure 3***D) using the modeled locations as the actual class and the detected locations as the predicted class to identify true positives (TP), false negatives (FN), and false positives (FP).

Detection tolerance reveals the tradeoff between recall and precision

Recall and precision were evaluated for the four model permutations. Recall, as the ratio of detected TPs to ground truth TPs, provides a measure for the 'missed' cluster locations. Precision, as the ratio of the number of detected TPs to all detected sites (TPs and FPs), measures the impact of false positives. Higher values indicate better performance in both cases.

For each simulated imaging plane, modeled RyR clusters were considered ground truths if their distance from the imaging plane was below a threshold we refer to as 'detection tolerance' (***Figure 4***). Recall and precision were evaluated as a function of variable detection tolerance rather than selecting an arbitrary fixed value. This approach highlighted the inherent trade-off between recall and precision across the models (***Figure 5***).

Clusters located on or very near the imaging plane were the most likely to affect the signal and be detected by the algorithm, as indicated by the consistently high recall at low detection tolerance. At low detection tolerance, clusters detected by CaCLEAN located just outside of this arbitrarily narrow window registered as false positives, producing low precision. Conversely, with a very wide definition of the detection tolerance, recall drops, as far away ground truth clusters do not strongly contribute to the signal at the imaging plane. Precision approaches an asymptotic maximum, as the imaged space becomes saturated with potential far-field ground truth options, thus dropping the number of false positives. The precision asymptote appears to be 1 except in the densely-packed with mitochondrial barriers case, where additional false positive events resulted in a slight drop to 0.95.

Inter-cluster spacing has a greater impact on CaCLEAN performance than mitochondrial diffusion barriers

The intersection of the recall and precision curves identifies the detection tolerance at which the number of false positives is equivalent to the number of false negatives (and therefore the 'correct'

number of clusters is still predicted). While there may be applications where optimising for recall or precision alone may be appropriate, this intersection point was a useful indicator of general performance. The intersection point values are indicated by the dashed lines in ***Figure 5*** and ***Figure 6***. Without mitochondria, in the low cluster density case recall = 0.83 ± 0.049 and precision = 0.83 ± 0.075 at a detection tolerance of 640 nm; in the high cluster density case recall = 0.70 ± 0.079 and precision = 0.70 ± 0.112 at a detection tolerance of 270 nm.

Inter-cluster spacing was found to have a greater impact on the performance of CaCLEAN than the presence of mitochondria. With mitochondria acting as barriers to diffusion, in the low cluster density case recall = 0.82 ± 0.059 and precision = 0.82 ± 0.073 at a detection tolerance of 610 nm; in the high cluster density case recall = 0.69 ± 0.079 and precision = 0.69 ± 0.091 at a detection tolerance of 280 nm. Mean recall and precision values for each model permutation (solid lines in ***Figure 5***) were further analysed to produce a precision-recall curve (***Figure 6***).

Discussion

We developed a computational model of the complex environment of Ca2+ diffusing into the intracellular space of a cardiomyocyte. Processing the reaction-diffusion model results to simulate confocal fluorescence microscopy data allowed for quantitative assessment of the performance of detection of Ca2+ release sites with CaCLEAN against known ground truth values in the context of realistic cellular physics. Statistical classification identified true positives, false positives, and false negatives[1]; enabling analysis in terms of recall (sensitivity, hit rate, or true positive rate) and precision (positive predictive value).

A key variable in the performance analysis was the window for the definition of the actual class positives in the through-imaging-plane direction, which we defined as 'detection tolerance' as illustrated in ***Figure 4***. Simulating confocal microscopy data from the FE model produced two-dimensional images, collapsing the through-imaging-plane direction at each time step. Parameterising algorithmic performance in terms detection tolerance provided a more complete picture and avoided an arbitrary choice of this key value.

Furthermore, detection tolerance is of practical interest to biologists or others interested in applying CaCLEAN to their data. The results of ***Figure 5*** quantify the inherent trade-off between precision and recall as a function of detection tolerance. This also allowed for identification of the 'intersection point' as a general performance measure: where precision is equal to recall and the number of false positives is equal to the number of false negatives, producing the correct number of true detected clusters overall.

We investigated the impact of cluster spacing on CaCLEAN detection performance by analysing two cluster distribution types. In the 'high cluster density' case, cluster locations at each z-disk were defined based on statistical analysis of cluster distributions from immuno-labeled confocal images and applied to admissible locations bordering mitochondria and myofibrils segmented from electron tomography data using a previously published method (***Rajagopal et al., 2015***). This simulated a case where all available RyR clusters fired during the 30 ms period modeled. In the 'low cluster density' case, distributions of clusters were similarly generated but with an additional constraint of a minimum spacing of 1 μm between all clusters within a given z-disk. The number of clusters was therefore also reduced to allow for this constraint. These distribution types form high and low bounds on distribution densities, while also revealing the impact of the stated 1 μm minimum cluster spacing requirement on detection with CaCLEAN.

Cluster spacing had a significant impact on both the performance of CaCLEAN and the detection tolerance at which the algorithm performed best. At the intersection point of the 'with mitochondria' cases, detection recall and precision were 0.82 at 610 nm in the low cluster density case versus 0.69 at 280 nm in the high cluster density case. In contrast, for the low cluster density results at the

[1] True negatives were not considered in this application, as they would represent the set of all remaining locations that were neither modeled nor detected.

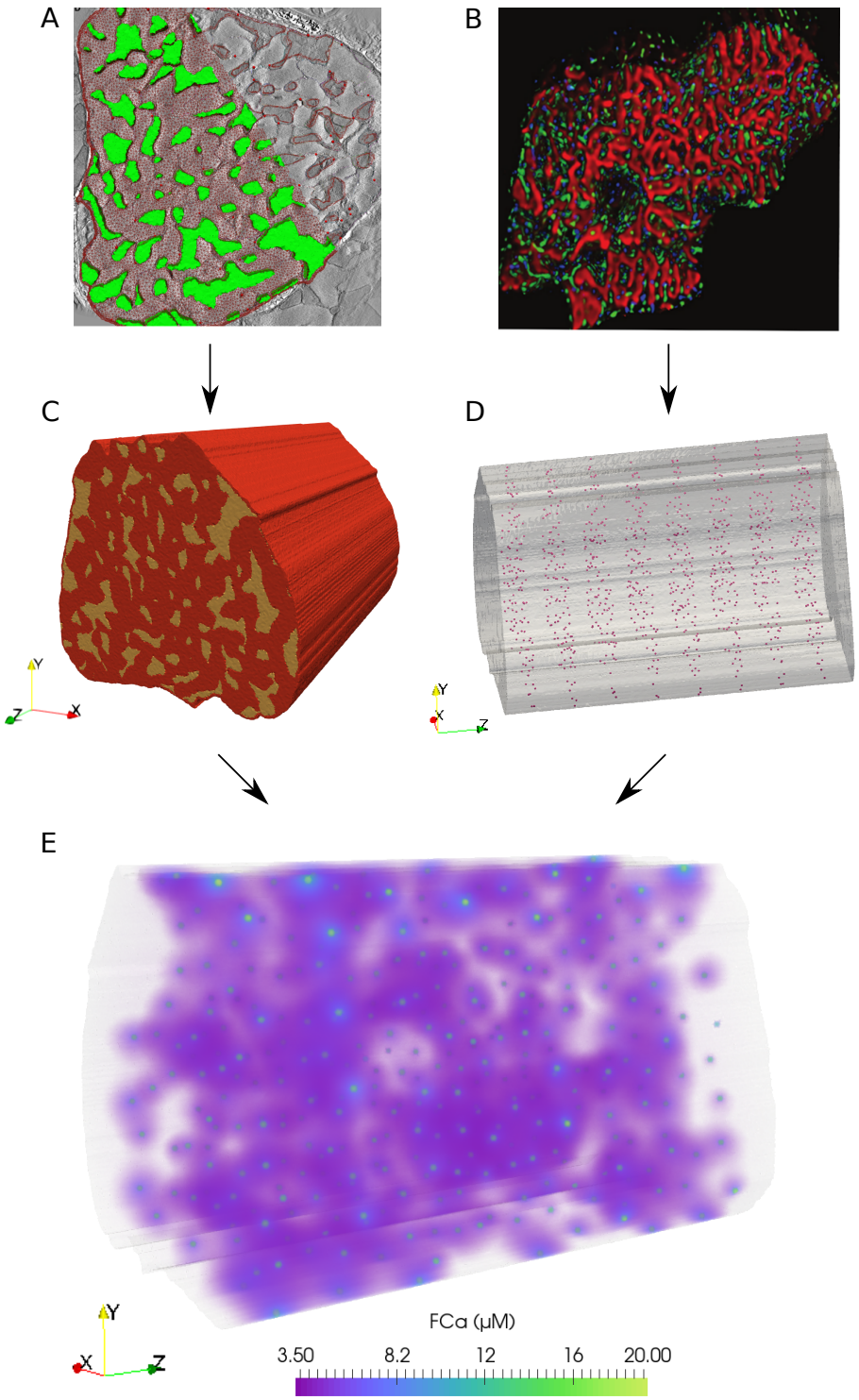

Figure 1. Finite element model of Ca2+ reaction-diffusion in an eight-sarcomere section of a cardiomyocyte. (A) From an electron tomography imaging stack, myofibril and mitochondria (portions highlighted in green) regions were segmented from a slice at the depth of a z-disk. (C) This geometry was extruded 16 μm (in the direction shown as z here) to create a three-dimensional eight-sarcomere model. Mitochondrial regions shown in yellow; red volume indicates the myofibrillar and cytosolic region. (B) Statistical analysis of immuno-labeled microscopy data (RyR clusters shown in green) was used to determine inter-cluster spacing distributions. (D) RyR cluster locations in the model were defined at mitochondrial and myofibrillar border regions based on statistical spacing distributions. (E) A reaction-diffusion finite element model simulates the release of calcium from the RyR clusters during the rising phase (first 30ms) of the calcium transient. Volume rendering of the fluorescence-bound calcium (FCa) fieldshown at t = 15ms.

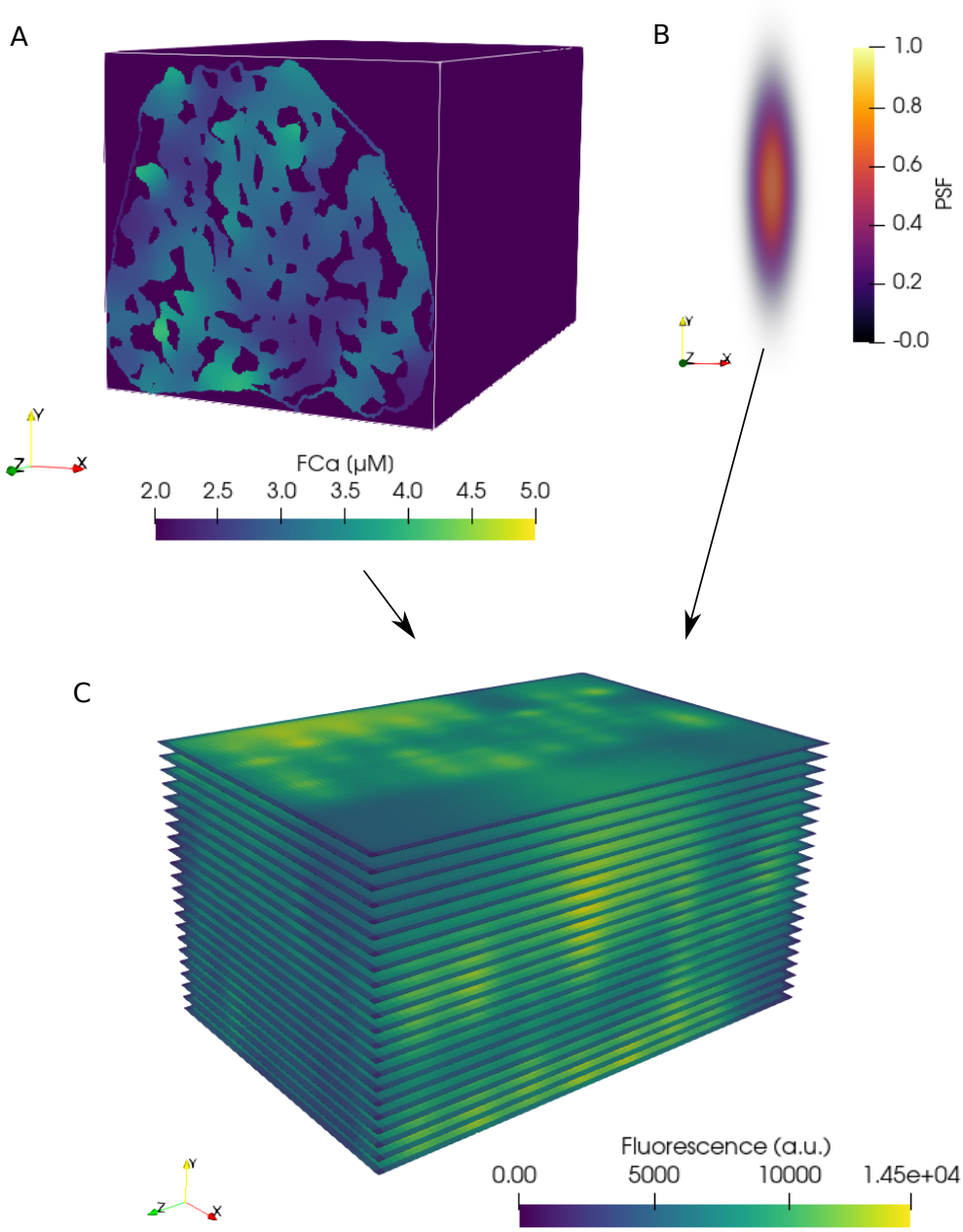

Figure 2. Simulation of confocal fluorescence microscopy images from FE model results. (A) FE FCa field data (see ***Figure 1***E) interpolated onto a regular grid with 53.75 nm resolution in each coordinate direction. Three-dimensional convolution of the interpolated FCa data with a (B) point spread function (PSF) produces blurring typical of confocal fluorescence microscopy data. (C) Blurred data resampled at a resolution of 215 nm within the 22 simulated two-dimensional imaging planes in the volume. A and C are shown at a single time point, t = 15 ms.

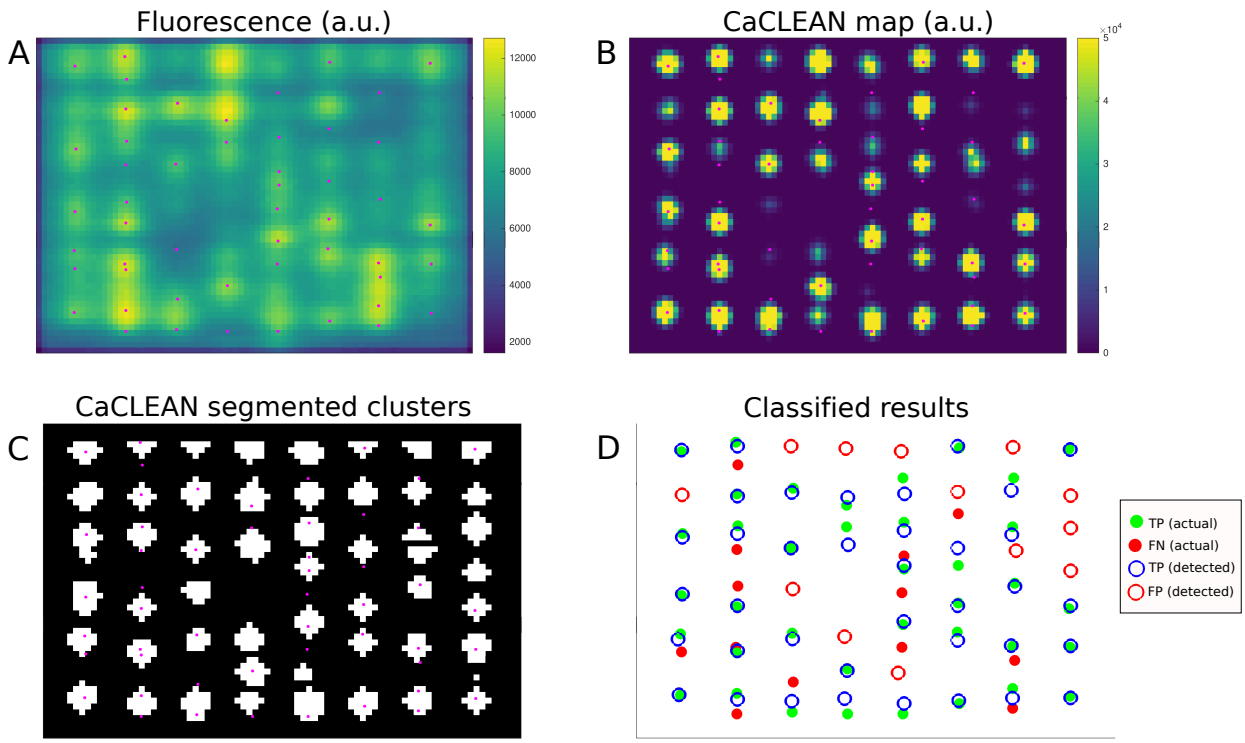

Figure 3. Example of CaCLEAN detection and classification against modeled locations. (A) Simulated confocal fluorescence microscopy image at t=15 ms for the densely packed cluster case (N=123 per z-disk) with mitochondria. This represents one slice from the middle of the stack shown in ***Figure 1***H. Modeled RyR cluster center locations within 280 nm of the imaging plane shown in magenta (also in B and C). (B) CaCLEAN map of the fluorescence signal. (C) Segmented clusters detected by CaCLEAN. (D) Statistical classification of detected cluster locations versus actual modeled locations. In this case recall = 0.68 and precision = 0.68, representing an 'intersection point' detection tolerance, as described further below.

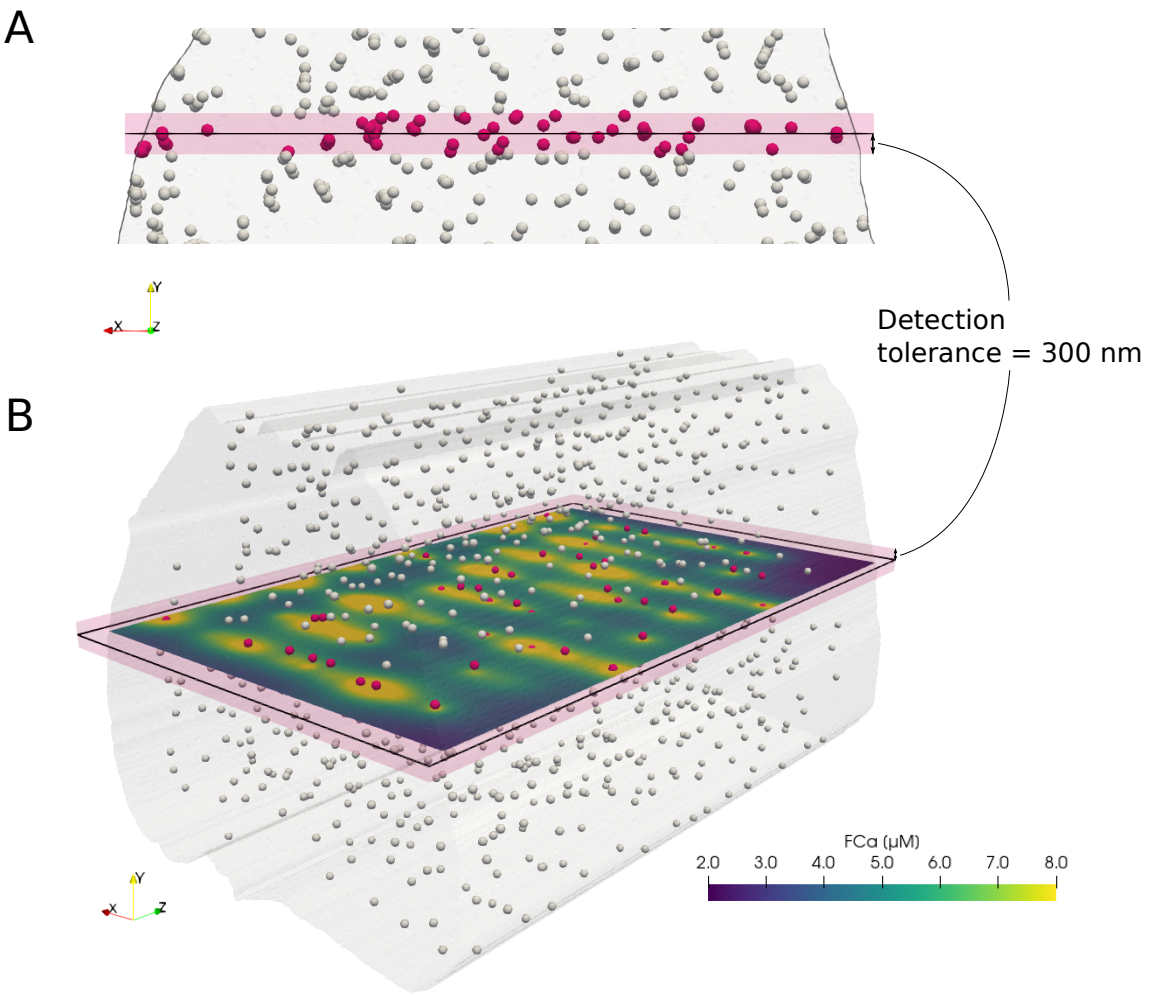

Figure 4. Illustration of the detection tolerance parameter. The detection tolerance parameter defines the distance from the simulated imaging plane a RyR cluster center are defined as an actual true positive. RyR clusters with centers located within the example 300 nm detection tolerance are shown in magenta, the detection tolerance window is shown in pink, and clusters located outside the detection tolerance window are shown in white. (A) x-y axis view, oriented perpendicular to the simulated imaging plane. (B) Oblique view of the simulated imaging plane, with the FCa model results shown at t = 15ms. This example represents a single slice from the high cluster density without mitochondria case (Case 1).

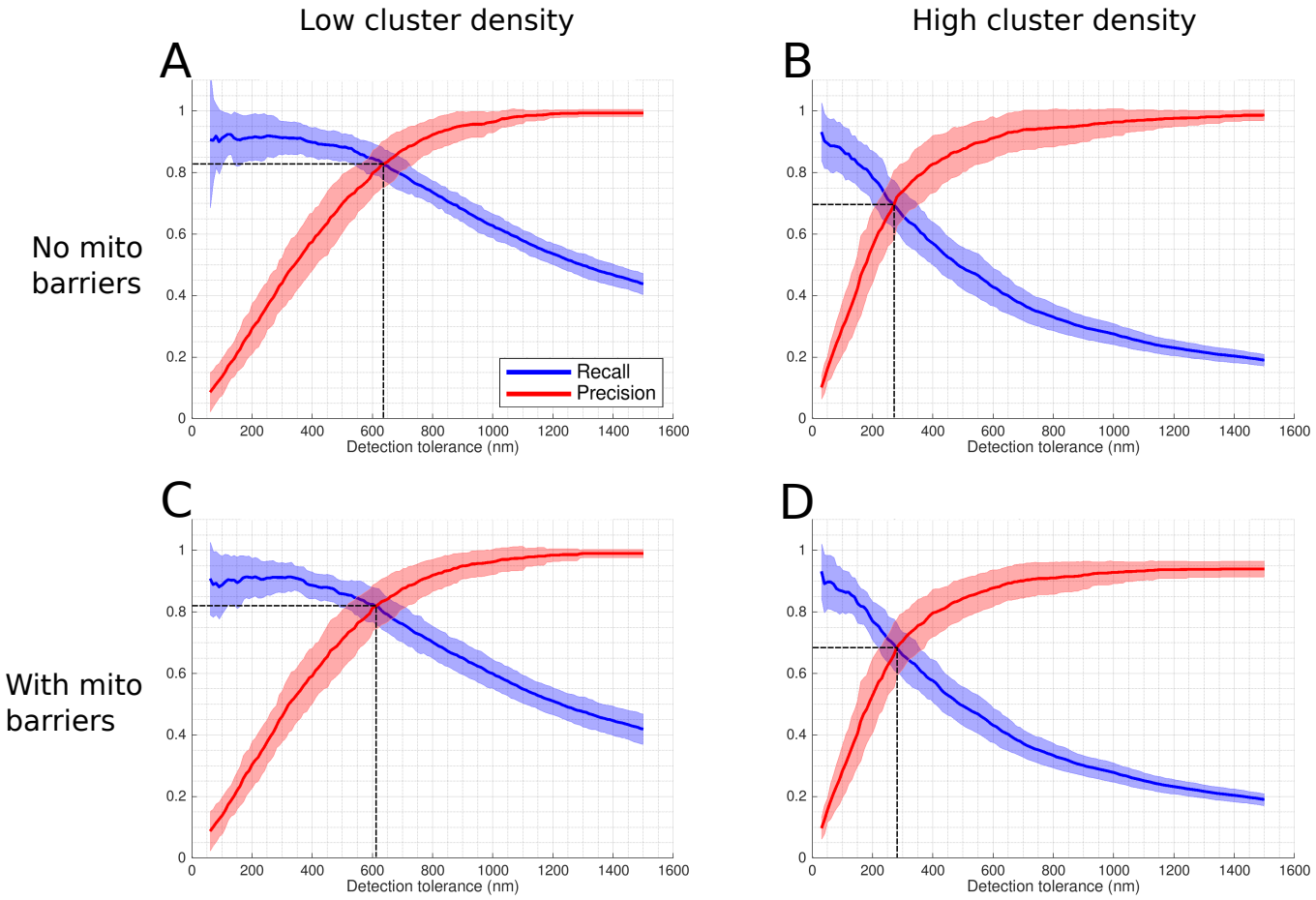

Figure 5. Recall and precision of CaCLEAN applied to simulated microscopy data. Recall and precision shown as a function of actual modeled RyR cluster center distances from the simulated imaging plane. In each case, 22 images were simulated with equidistant spacing through the model volume. Shaded regions indicate one standard deviation of recall and precision values within the group of 22 image slices. The effect of mitochondria acting as barriers to diffusion and the effect of inter-cluster spacing were examined, producing four permutations. (A) A minimum spacing of 1 μm is enforced between modeled clusters, no mitochondria present in the volume (resulting in a continuous domain across the mitochondrial regions). (B) Cluster spacing is determined by statistical analysis of RyR cluster distributions from immuno-labeled super-resolution microscopy data, no mitochondria present in the volume. (C) A minimum cluster spacing of 1 μm is enforced between modeled clusters, mitochondrial regions are subtracted from the volume, acting as barriers to diffusion. (D) Cluster spacing is determined by statistical analysis of RyR cluster distributions from immuno-labeled super-resolution microscopy data, mitochondrial regions are subtracted from the volume, acting as barriers to diffusion. Dashed black lines used to indicate values at 'intersection points', where recall = precision.

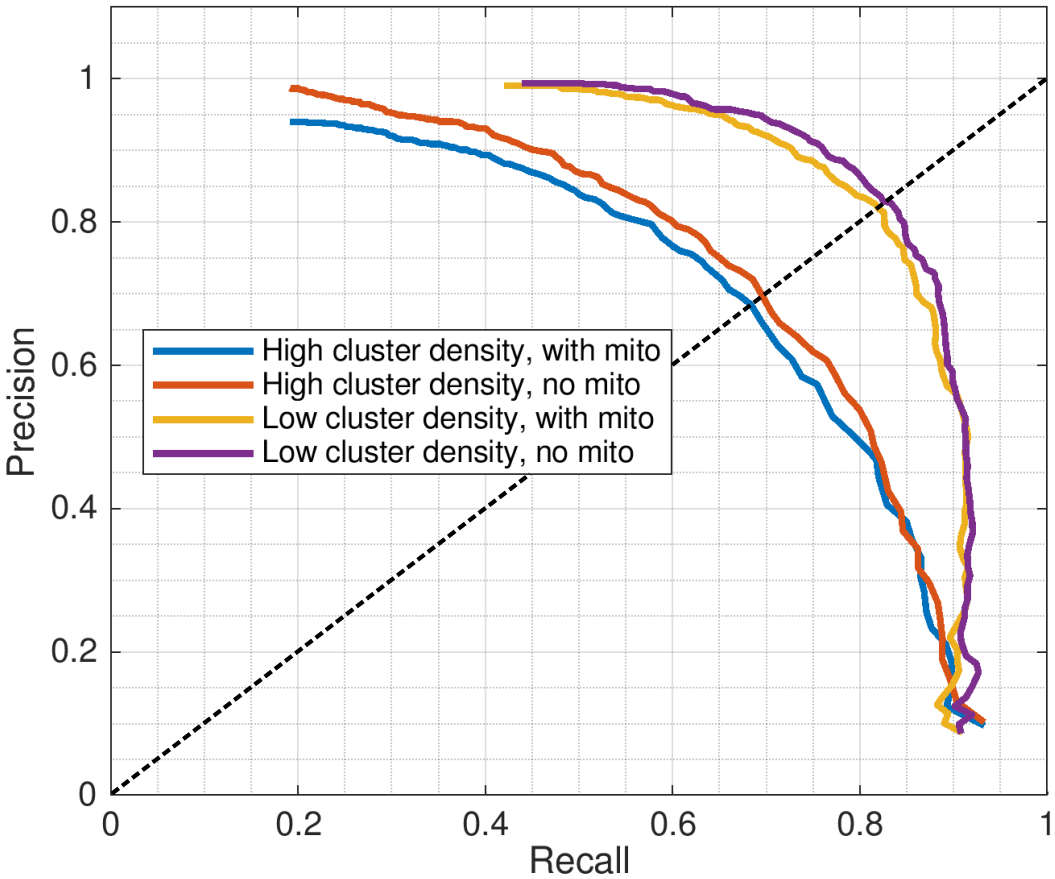

Figure 6. Precision-recall curve for CaCLEAN in four models. Recall and precision mean values from results shown in ***Figure 5*** plotted as a precision-recall curve. Dashed line indicates intersection point, where recall = precision.

high cluster density intersection point detection tolerance of 280 nm, precision = 0.43 indicating more false positives than true positives. For usefully accurate detection, it is therefore important for an interested user to consider the density of the events being detected and how far from the imaging plane these events may be located (i.e., the detection tolerance). Those interested in using CaCLEAN to reconstruct full three-dimensional maps of all clusters should also be aware of how far away from the imaging plane clusters detected by the algorithm are likely to be when choosing a slicing depth for reconstruction.

The presence of mitochondria in the presented models was found to have a marginal but consistent negative impact on both recall and precision in CaCLEAN. This was most pronounced in the high cluster density case, as evident from the precision-recall analysis (***Figure 6***). We therefore hypothesize that structural heterogeneity due to the presence of subcellular structures (e.g., mitochondria, nucleus, transverse tubules, z-disks, etc.) is unlikely to have a major impact on detection of point sources using CaCLEAN or related algorithms under the imaging conditions simulated here.

The results here (particularly ***Figure 5*** and ***Figure 6***) have been provided as a reference for potential users of CaCLEAN. The model and the simulated imaging data produced by it could also serve as a testing and validation platform for further improving CaCLEAN or other approaches seeking to identify RyR clusters by serving as a training set for improved detection or segmentation. Finally, this study highlights how computational methods may be used to establish ground truth values that may not otherwise be experimentally available.

Materials and methods

Finite element model of reaction-diffusion in a half-sarcomere

The reaction-diffusion finite element (FE) model here builds on a previous FE model of a half-sarcomere (***Rajagopal et al., 2015***). From electron tomography (ET) images of adult rat ventricular myocytes, a three-dimensional axial region with a thickness of approximately 0.875 μm was segmented. This region represented approximately half of a single sarcomere, with the z-disk a plane through the center of the thickness of the domain. The region was approximately 11 μm in diameter, varying with the segmented surface.

From this half-sarcomere image stack, the central slice representing the level of the z-disk was extracted and regions representing myofibrils and mitochondria were manually segmented. This two-dimensional slice was then extruded 16 μm to create a three dimensional volume.

Two configurations were considered to assess the impact of mitochondria: one in which the interior of the modeled domain is a homogeneous material continuum and one in which the regions representing mitochondria were subtracted from the myofibrillar and cytoplasmic domain. The latter case was based on the assumption that the calcium buffering activity of mitochondria is negligible.

Ryanodine receptor (RyR) locations were determined algorithmically, using a spatial statistics method based on nearest neighbour distances of experimentally-derived RyR locations (***Rajagopal et al., 2015***). These distributions were determined from confocal images of left ventricular cardiomyocytes of a healthy adult male Wistar rat using multiple passes of a band-pass filter detector, following the technique described by ***Soeller and Cannell*** (***2002***). The method also limits the admissible locations of RyR clusters to segmented regions bordering myofibrils, mitochondria, and the sarcolemma (i.e., RyR clusters were not placed inside these organelles).

To evaluate the influence of spacing on the RyR cluster detection performance of CaCLEAN, two sets of constraints on the RyR distributions were considered: (1) RyR clusters were assigned following ***Rajagopal et al.*** (***2015***), with locations based directly on statistical analysis of experimental data and with the total number of RyR clusters N=123 per z-disk (984 total); (2) a minimal distance constraint of 1 μm between RyR cluster centers was enforced and the total number of clusters was reduced to N=51 per z-disk (408 total) to allow for this constraint. Linear tetrahedral meshes were constructed on these domains, consisting of: (1) 1436943 nodes, 8222684 elements; and (2)

1318942 nodes, 7504655 elements respectively. These meshes included further refinement in the regions containing and surrounding the modeled RyR locations.

Spherical regions 100 nm in radius were defined around nodes nearest to the determined location for each RyR cluster. Nodes lying within this sphere were prescribed density amplitudes exponentially decreasing as a function of the square of their radial position from the central node. RyR cluster release times were sampled from an exponential distribution with a characteristic decay constant of 6.7 ms, following the findings of ***Wang et al.*** (***2001***).

Further details on the reaction diffusion equations for the buffers modeled and the ordinary differential equation model describing release of Ca2+ from RyR clusters have been previously reported (***Rajagopal et al., 2015***).

Simulation of confocal fluorescence signals from FE model results

To simulate confocal fluorescence results, the irregularly distributed node-based fluorescence fields from the FE model was first interpolated onto a regular grid at a resolution of 107.5 nm in each direction. The data was temporally sampled at 5 ms intervals over the simulated time period of 30 ms, producing simulated imaging data for 7 timesteps. Nodal positions within mitochondria in the 'with mitochondria' permutations were ascribed the initial and background value FCa = 2.08. Discrete natural neighbor (Sibson) interpolation (***Park et al., 2006***) was chosen for this task on the basis that it can be used to generate regularly-spaced three-dimensional data, scales well for large datasets, and does not require additional parameterisation (as opposed to other multivariate interpolation methods like Kriging or inverse-distance weighting). The implementation used was version 1.7 of the naturalneighbor python package, available from the Python Package Index under the MIT license.

A point spread function (PSF) was generated as a normalised function of a multivariate Gaussian distribution applied in three dimensions (see ***Figure 2***B). These distributions had a full width at half maximum (FWHM) of 410 nm in x and y and 1800 nm in z (where the z-axis represents the through-imaging-plane direction, shown as 'y' in ***Figure 2***B.). The values were based on reported estimates of the dimensions of a PSF from a Visitech confocal microscope (***Plumb et al., 2015***). The resolution of the PSF image was chosen to be the same as the interpolated model data (53.75 nm in each direction). A small amount of noise (SNR = 100) was also added to the data after convolution with the PSF.

The interpolated model imaging data was then convolved with the PSF in three dimensions using the SciPy convolve algorithm from the signal processing module. The resulting grid was then downsampled to a pixel resolution of 215 nm, following the resolution of the original CaCLEAN paper (***Tian et al., 2017***). Representative slices were sampled along the y-axis of the FE model, producing 20 two dimensional simulated microscopy images for each of the four reported model permutations.

Application of CaCLEAN to simulated fluorescence data

The CaCLEAN algorithm was obtained from the author's GitHub repository: https://github.com/qhtian/CaCLEAN. The Matlab-based scripts were run using Matlab version R2017b. The function CICRcleanSimp was used to generate the CaCLEAN release map and the function CRUProps was used to segment the release map into individual calcium release units (CRUs).

Classifying and quantifying performance of CaCLEAN

A statistical classification approach was used to assess the performance of RyR cluster detection using CaCLEAN. Modeled cluster centers were considered the actual true class, while CaCLEAN detection results were considered the predicted class. Detected RyR cluster sites were defined as determined by the CaCLEAN CRUProps function, which segments cluster regions using Matlab's built-in watershed algorithm and identifies centroids of segmented regions.

For each modeled cluster location, a true positive (TP) classification was assigned if an actual (modeled) cluster location was within (or within a tolerance of one pixel of) an available segmented CaCLEAN cluster region. When more than one actual cluster fell within a predicted region, the actual with the closest distance to the predicted centroid was marked as TP. After classification as TP, the associated CaCLEAN-detected site would be removed from the list of available matches. After iterating through the actual modeled clusters, remaining unmatched modeled clusters were classified as false negatives (FN) and remaining unmatched CaCLEAN-detected sites were classified as false positives (FP).

Two statistical measures were considered: recall and precision. Recall (also known as sensitivity, hit rate, or true positive rate) was defined such that

$$\text{Recall} = \frac{\text{TP (predicted)}}{\text{TP (actual)}}. \tag{1}$$

Recall therefore gives the fraction of actual clusters that were detected by CaCLEAN. Precision (also known as positive predictive value) was defined such that

$$\text{Precision} = \frac{\text{TP (predicted)}}{\text{TP (predicted)} + \text{FP (predicted)}}. \tag{2}$$

Precision therefore identifies the fraction of the detected clusters that were correct (not false positives). In both cases, higher values indicate better performance.

References

Bers DM. Cardiac excitation–contraction coupling. Nature. 2002 Jan; 415:198–205. http://www.nature.com/articles/415198a, doi: 10.1038/415198a.

Hou Y, Jayasinghe I, Crossman DJ, Baddeley D, Soeller C. Nanoscale analysis of ryanodine receptor clusters in dyadic couplings of rat cardiac myocytes. Journal of Molecular and Cellular Cardiology. 2015 Mar; 80:45–55. http://www.sciencedirect.com/science/article/pii/S0022282814004258, doi: 10.1016/j.yjmcc.2014.12.013.

Högbom JA. Aperture Synthesis with a Non-Regular Distribution of Interferometer Baselines. Astronomy and Astrophysics Supplement Series. 1974 Jun; 15:417. http://cdsads.u-strasbg.fr/abs/1974A%26AS...15..417H.

Park SW, Linsen L, Kreylos O, Owens JD, Hamann B. Discrete Sibson Interpolation. IEEE Transactions on Visualization and Computer Graphics. 2006 Mar; 12(2):243–253. http://dx.doi.org/10.1109/TVCG.2006.27, doi: 10.1109/TVCG.2006.27.

Plumb K, Elaz S, Pelletier V, Kilfoil ML. Automated three-dimensional single cell phenotyping of spindle dynamics, cell shape, and volume. arXiv:150400714 [physics]. 2015 Apr; http://arxiv.org/abs/1504.00714, arXiv: 1504.00714.

Rajagopal V, Bass G, Walker CG, Crossman DJ, Petzer A, Hickey A, Siekmann I, Hoshijima M, Ellisman MH, Crampin EJ, Soeller C. Examination of the Effects of Heterogeneous Organization of RyR Clusters, Myofibrils and Mitochondria on Ca2+ Release Patterns in Cardiomyocytes. PLOS Computational Biology. 2015 Mar; 11(9):e1004417. http://journals.plos.org/ploscompbiol/article?id=10.1371/journal.pcbi.1004417, doi: 10.1371/journal.pcbi.1004417.

Soeller C, Cannell MB. Estimation of the Sarcoplasmic Reticulum Ca2+ Release FluxUnderlying Ca2+ Sparks. Biophysical Journal. 2002 May; 82(5):2396–2414. http://www.sciencedirect.com/science/article/pii/S0006349502755847, doi: 10.1016/S0006-3495(02)75584-7.

Soeller C, Crossman D, Gilbert R, Cannell MB. Analysis of ryanodine receptor clusters in rat and human cardiac myocytes. Proceedings of the National Academy of Sciences. 2007 Sep; 104(38):14958–14963. http://www.pnas.org/content/104/38/14958, doi: 10.1073/pnas.0703016104.

Tian Q, Kaestner L, Schröder L, Guo J, Lipp P. An adaptation of astronomical image processing enables characterization and functional 3D mapping of individual sites of excitation-contraction coupling in rat cardiac muscle. eLife. 2017 Nov; 6:e30425. https://elifesciences.org/articles/30425, doi: 10.7554/eLife.30425.

Wang SQ, Song LS, Lakatta EG, Cheng H. Ca^{2+} signalling between single L-type Ca^{2+} channels and ryanodine receptors in heart cells. Nature. 2001 Mar; 410(6828):592–596. http://www.nature.com/articles/35069083, doi: 10.1038/35069083.

Williams GSB, Boyman L, Chikando AC, Khairallah RJ, Lederer WJ. Mitochondrial calcium uptake. Proceedings of the National Academy of Sciences. 2013 Jun; 110(26):10479–10486. http://www.pnas.org/content/110/26/10479, doi: 10.1073/pnas.1300410110.